To appear in Astronomical Journal, 999

Simultaneous Polarimetry and Photometry of the Young Stellar Object R Mon[1]

M. Matsumura
Faculty of Education, Kagawa University,
Saiwai-cho 1-1, Takamatsu 760-8522, Japan

and

M. Seki[2] and K. Kawabata[2,3]
Astronomical Institute, Tohoku University, Sendai 980-8578, Japan

ABSTRACT

Linear polarization and flux of the young stellar object R Mon were observed simultaneously at 7 bands in the optical wavelength from 0.36 to 0.76 μm in 1991-1997. During the observational period, the V magnitude of R Mon changed by about 0.7 mag in a diaphragm of 18$''$. We have found a strong positive correlation between the degree of linear polarization p and the V magnitude, and that the coefficient of correlation is 0.92 for the data in 1993-1997. The values of p and V in 1991-1992 did not follow this correlation. The colors ($B-V$, $V-R_c$, and R_c-I_c) are also found to increase with the V magnitude in the whole observational period. However, in 1991 when the object was in the faintest phase, only the color $U-B$ decreased. These correlations are similar to those observed in other Herbig Ae/Be stars. The position angle θ of the linear polarization also shows significant variation with time, though the correlation between θ and other quantities is weak.

The observed correlations between magnitude, colors, and polarization degree can be explained by the combination of extinction by the clouds orbiting around R Mon and scattering by diffusely surrounding medium, as originally proposed by Grinin 1988 for Herbig Ae/Be stars. Since the time scale of variation is short ($\approx$10 days), the orbiting clouds should be in the vicinity, i.e. $\lesssim$10 AU, of the star. The extinction by those clouds less depends on wavelength than that observed in the diffuse interstellar medium. The size of grains in the clouds may be larger than those in the diffuse

[1]Based on observations obtained at the Dodaira Observatory, which is operated by the National Astronomical Observatory of Japan.

[2]Visiting Astronomer, Dodaira Observatory.

[3]National Astronomical Observatory, Mitaka, Tokyo 181-8588, Japan

interstellar clouds. Our Mie calculations show that the radius of grains may be in the range from 0.08 to 0.50μm. Alternatively, if the clouds are dense and opaque, 'gray' extinction may occur and explain the observation.

Subject headings: stars: pre-main sequence — stars: individual(R Mon) — circumstellar matter — techniques: polarimetric — techniques: photometric

1. INTRODUCTION

The variable star R Mon is one of the most highly polarized objects among Herbig Ae/Be stars (Herbig and Bell 1988, Thé et al 1994), located at a distance of about 800 pc (Walker 1956, Close et al. 1997). This object is associated with a cometary reflection nebula, NGC 2261 or Hubble's nebula, which also shows variabilities with time in brightness and its appearance (e.g. Lightfoot 1989). Based on the high resolution adaptive optics images at the near-infrared, Close et al. 1997 has found that R Mon is a $0.7''$ binary star.

Both R Mon and NGC 2261 show large linear polarization amounting to $\approx$10-15% in the optical wavelength (Khatchikyan 1958, Razmadze 1959, Hall 1964, Hall 1965, Zellner 1970, Garrison and Anderson 1978, Jones and Dyck 1978, Vrba et al. 1979, Aspin et al. 1985, Warren-Smith et al. 1987, Scarrott et al. 1989, Matsumura and Seki 1995). Electric vectors in the polarization map make a centrosymmetric pattern in the outer region of the nebula, while they align in a certain direction near the star. The centrosymmetric pattern can be explained by single scattering of stellar light. However, the mechanism of the aligned pattern is less clear: one may explain it by dichroic extinction due to aligned nonspherical grains (Aspin et al. 1985, Minchin et al. 1991). This is the same mechanism for the interstellar polarization. However, Bastien and Ménard 1990 pointed out several difficulties in this model. The most widely accepted explanation is that the observed polarization results from multiple scattering of light within circumstellar disk and/or envelopes (Ménard et al. 1988, Bastien and Ménard 1988, Fischer et al. 1994, Fischer et al. 1996, Whitney and Hartmann 1992, Whitney and Hartmann 1993).

Many Herbig Ae/Be stars show time variations in magnitude and colors, and these quantities correlate with each other (e.g. Thé et al 1994, Grinin 1994, for reviews). When the star decreases in brightness it first becomes redder, and it turns to be bluer after reaching a certain magnitude. This is called as the 'bluing effect'. Grinin 1988 explained the bluing effect by the combination of extinction and scattering of light, assuming that the matter around the star is distributed inhomogeneously. If the optically thick clouds begin to obscure the star, the color becomes redder by the effect of extinction. However, at the deepest obscuration, the optically thick clouds act as a 'natural coronograph', and the blue light scattered by more diffuse cloud become visible. Thus, one can explain the observed variations of flux and colors. In this paper, we refer to this model as the 'eclipsing model'.

Grinin 1988 has pointed out that simultaneous polarimetry and photometry are particularly important to examine the validity of the eclipsing model, and predicted a positive correlation between the polarization degree and the magnitude. Subsequent simultaneous observations showed that many Herbig Ae/Be stars can be explained by this model, though some other objects cannot (e.g. Thé et al 1994, Hutchinson et al. 1994). Since the number of well-studied Herbig Ae/Be stars seems limited at present, we need more extensive simultaneous photo-polarimetry, to understand the mechanism of variation in detail.

We made simultaneous photometry and polarimetry of R Mon from 1991 to 1997, with a multi-channel photo-polarimeter at the Dodaira Observatory of the National Astronomical Observatory of Japan, to study the mechanisms of the optical polarization and the photometric variation. Although it is well known that R Mon shows significant variability both for flux and polarization, simultaneous observation of them seems rare as far as we know. In a previous paper (Matsumura and Seki 1995), we reported the results on polarization in 1991-1993, while in this paper we present not only polarimetric data but also photometric ones from 1991 to 1997. Our results show that the V magnitude varies by about 0.7 mag in a diaphragm of $18''$, and the color and the degree of linear polarization also vary with time. The position angle of linear polarization changed by about 20 degrees during the observational period, but was only weakly correlated with other quantities. The position angle depends on wavelength and this dependence seems to last for decades. On the basis of these results, we discuss the mechanism of variability, the light scattering process, and the size distribution of grains in this object.

2. OBSERVATION

Throughout this study, we have used the multi-channel photon-counting polarimeter attached to an 91cm telescope at Dodaira Observatory. It uses a rotating achromatic half-wave plate and a Wollaston prism as polarizer. The stellar light into the polarimeter first passes the polarizer, then it is divided by dichroic mirrors and passes color filters, and finally it is guided to 8 photomultipliers which cover the wavelength from 0.3 to 1.1 μm (Kikuchi 1988). The effective wavelength λ_{eff} for each channel is given in Appendix. For the longest waveband ($\lambda_{eff} = 0.88\mu$m), we could not obtain any reliable data, because the sensitivity of the photomultiplier for this band was too low for R Mon.

We have observed R Mon with two concentric circular focal-plane diaphragms, whose diameters are $18''(\phi_1)$ and $36''(\phi_2)$ on sky. At a distance of 800 pc for R Mon (Walker 1956, Close et al. 1997), those angular diameters correspond to 14400AU and 28800AU in the linear scale, respectively. Since R Mon shows a semi-stellar image ($\approx 5''$) and NGC 2261 is more extended, we used these diaphragms to obtain the information on the semi-stellar image and its nearest surrounding areas. The typical integration time in one series of observation was 267 seconds for ϕ_1 and 133 seconds for ϕ_2, i.e. 400 seconds with using both diaphragms. We repeated it several times in one night. The sky background was estimated at the position $6'21''$ south of R Mon where any nebulosity was found neither on O nor on E plates of the Palomar Observatory Sky Survey.

We reduced the polarimetric data as described below. Instrumental polarization was estimated from the observation of non-polarized standard stars. The position angle for the channel 4 ($\approx$ V band) was calibrated by observing strongly polarized standard stars. We usually observed 9 Gem as a polarized standard. This star is relatively near R Mon on sky among the polarized stars listed in Serkowski 1974. For this star, however, variabilities were reported (Hsu and Breger 1982). We thus compared our data for 9 Gem with those for other polarized standards, and found that the variation in position angle for 9 Gem was less than a few degrees (Matsumura et al. 1998). The position angles of the other channels were corrected by observing bright stars through a Glan-Taylor prism. Depolarization factors were obtained on the assumption that the light through the Glan-Taylor prism was fully polarized, and were applied to all the data.

Comparative photometry of R Mon was made with a nearby star, SAO 114210 (=HD 261416, we refer this star as C_1), and this star was also photometrically compared with another nearby star HD 251389 (=C_2). No significant temporal variation was found in the difference between all the magnitudes and colors for C_1 and C_2. Therefore, both C_1 and C_2 should not be variable and they are suitable for comparison stars. For C_1, we have also made comparative photometry to photometric standard stars (Moffett and Barnes 1979). The magnitudes at 7 bands were linearly transformed to those in the standard system (see Appendix). The final results of magnitude and colors for C_1 and C_2 are presented in Table 1.

The colors of C_1 are consistent with that C_1 is an A0 star (according to the HD catalog) with negligible color excess. Even if we include the uncertainty, the $B-V$ color is at most about 0.03 mag, and then the color excess E_{B-V} should be less than 0.03 mag, because the intrinsic color of A0 star is 0.00 mag by the definition. Our polarimetry of C_1 shows that the degree of linear polarization is less than 0.1% at V band. Thus the foreground extinction A_V for C_1 is less than 0.1 mag, if the empirical relations in the general diffuse interstellar medium, i.e. $p_V \lesssim 3A_V$ and $A_V \approx 3E_{B-V}$, hold for the line of sight to this star. If we neglect the foreground extinction for C_1 and we assume the absolute magnitude M_V of this star as 0.5 mag for an A0 star, the distance to C_1 is derived to be 610 pc. Since the distance to R Mon is estimated to be 800 pc (Walker 1956, Close et al. 1997), we can conclude that the amount of interstellar matter is quite small in the direction to these objects. We thus neglect the foreground effect in the following analysis.

3. RESULTS

3.1. Time Averaged Properties

In 1991-1997, we obtained polarimetric data in 29 nights, and photometric data in 26 nights. In 2 nights (JD=2448574 and 2450042), the temporal variation of telluric extinction was too rapid to obtain photometric data, and the photomultiplier for U band was not good in one night

(JD=2450108). As a first step, we calculate the averaged values of the observed data to know the fundamental properties of R Mon, though this object shows significant temporal variation. Table 2 presents the time averaged quantities over the 26 observations in the observed period. The results obtained with the small diaphragm (ϕ_1) and those with the large diaphragm (ϕ_2) are shown in the columns 2 and 3, respectively. The column 4 shows the values derived for the 'ring-shaped region' which is the region of ($\phi_2 - \phi_1$), surrounding the area of ϕ_1. The polarization degrees in ϕ_2 or in the ring-shaped region are smaller than those in ϕ_1, though the difference is relatively small, i.e. $\approx 1-2\%$. The position angles are about 3 degrees larger in ϕ_2 than in ϕ_1. These differences can be interpreted as due to the effect of the bright north-east arc in the nebula where the position angle is larger than that at the stellar image (e.g. see Warren-Smith et al. 1987). In our observation, the contribution from the north-east arc is greater in ϕ_2 than that in ϕ_1, and thus the position angle in ϕ_2 is larger than that in ϕ_1. From the data of two-dimensional polarization for R Mon, Aspin et al. 1985 calculated polarization with aperture diameters ranging from $5''$ to $30''$ in steps of $5''$ for B, V and R bands. They found that the difference in polarization degree is less than $\approx$1% in different aperture, and that in the position angle is less than $\approx 2-3$ degrees (Table 1 in Aspin et al. 1985). Both our results and those by Aspin et al. 1985 show that the effect of aperture size is less sensitive to the polarization properties. This is due to the fact that the contribution of flux from the outer region is relatively small, and that the polarization properties do not severely depend on the position in or around the stellar image. This property is particularly important in comparing the results by different observers with different instruments (Section 4.2). It should be noted, however, that the dependence of position angle on the aperture size is different between in Aspin et al. 1985 and in this paper. In Aspin et al. 1985 the position angle gradually *decreases* with increasing the aperture size from $5''$ to $30''$, while our results show it *increases* from $18''$ to $36\,''$. A possible explanation is that the brightness distribution in the nebula has changed and it has effect on the position angle in the larger aperture. The brightness of north-east arc seems less intensive in 1983 (Figs.1 and 7 in Aspin et al. 1985) than in 1985-1986 (Fig.1 in Warren-Smith et al. 1987). The contribution from the arc may be smaller in Aspin et al. 1985 than in this paper.

Figure 1 shows the polarization degree p and the position angle θ against the inverse wavelength λ^{-1}, where p and θ are averaged over each observational season. To study the wavelength dependence, we assume linear relations between p and λ^{-1}, and between θ and λ^{-1} as a first approximation:

$$p(\lambda) = p_V + a(1/\lambda - 1.82) \tag{1}$$

$$\theta(\lambda) = \theta_V + b(1/\lambda - 1.82) \tag{2}$$

where a and b are constants, and p_V and θ_V are the polarization degree and the position angle at the V band, respectively. Those parameters are calculated with our data, and listed in Table 2. The values of p_4 and θ_4 at channel 4 ($\lambda_{eff} = 0.53\mu m$) are nearly equal to the values obtained with the above equations (p_V and θ_V in Table 2), though the latter quantities have smaller errors and are more reliable. We have also attempted to make non-linear fitting with the Serkowski or the Wilking formula. However, we can not obtain any meaningful results, e.g. the wavelength at which the polarization reaches maximum is unreliably large with these formulae, and we have not used them.

Table 2 also shows observed colors in ϕ_1, ϕ_2 and the ring-shaped region. The colors are significantly bluer in the larger diaphragm, except for $U-B$. This can be interpreted as the effect of scattering being more significant in the outer region. Alternatively, the effect of extinction is more significant in the inner region, and this results in the redder colors in ϕ_1.

3.2. Temporal Variation

In this subsection, we examine only the data obtained with the small diaphragm ϕ_1, because the errors in the large diaphragm ϕ_2 or those in the ring-shaped region are relatively large. For example, in the V band, a typical error with ϕ_1 in one night observation is 0.02 mag, while that with ϕ_2 is 0.08 mag. Errors of colors are more than 0.1 mag. This results from the low signal-to-noise ratios by large contribution from the sky background in ϕ_2. We tabulate the results obtained with ϕ_1 in Table 3, which shows that all the quantities vary significantly with time.

Figure 2 shows the time dependence of $V, B-V$, p_V, and θ_V. The flux of the semistellar image (ϕ_1) of R Mon increased from 1991 to 1994, and then decreased (the filled circles in Fig.2a). The flux from the ring-shaped region shows a similar behavior to that for ϕ_1 (the open circles in Fig.2a). Other quantities, i.e. $B-V$, p, and θ_V, show more complex behaviors (Figs.2b-d). The position angle θ_V changed abruptly from the end of 1996 to the beginning of 1997. It is clearly demonstrated in Figure 3 with the Stokes parameters Q and U.

We calculated correlation coefficients between the quantities observed with ϕ_1 to see the mutual relations (Table 4). Strong correlations are found between p_V, V, and colors. The correlation between V and p_V is particularly strong (Fig.4), and the coefficient of correlation is 0.92 for JD$>$ 2449368 or after 1993.

To study variable properties, we have made a principal components analysis (PCA) using the 9 quantities tabulated in Table 4. From the correlation matrix, we calculate the eigenvalues and eigenvectors. Two large eigenvalues, or principal components, are obtained. The results show the 42% of variance in our data is attributed to the first largest component, and 24% to the second one. The first and second components y_1 and y_2 are expressed as

$$y_1 \approx 0.47V' + 0.41(B-V)' + 0.43(V-R_C)' + 0.41(R_C-I_C)' + 0.39P_V', \tag{3}$$

$$y_2 \approx 0.59(U-B)' + 0.39(R_C-I_C)' + 0.54\theta_V', \tag{4}$$

where the dash indicates that the quantities are subtracted by their means and are normalized by their standard deviations. The interpretation of the two components will be given in Section 4.4.

The correlation between $U-B$ and V is not linear (Fig.5a). When the object was relatively bright, linear relations were found between other colors and the V magnitude (Figs.5b-d).

However, when the object was faintest, the $U-B$ color turned blue. This phenomenon is similar to the 'bluing effect' observed in other Herbig Ae/Be stars.

3.3. Spatial Variation

The V-band magnitude in the ring-shaped region is compared with that in the small diaphragm ϕ_1 (Fig.6). As one may expect, the object was brighter in the large diameter ϕ_2 than in ϕ_1 (Table 2). However, it should be noted that the variation observed with the small diaphragm ϕ_1 was smaller (δV=0.7 mag) than that in the ring-shaped region (δV=1.0 mag). This property may be explained by multiple scattering in the vicinity of the star and is discussed in Section 4.4.

4. DISCUSSION

4.1. Variation of p_V and V

One of the most conspicuous properties of R Mon in our study is the strong correlation between the V magnitude and the degree of linear polarization p_V (Fig.4). A possible explanation of this correlation is that the observed polarization is due to dichroic extinction by aligned nonspherical grains. The polarization degree by this mechanism increases with the amount of extinction in the diffuse interstellar medium. The polarization degree observed in R Mon also increases with the V magnitude. However, a linear fit to the data gives a ratio of 9.8 %/mag in JD= 2449368-2450512 (the dotted line in Fig.4), and it is significantly larger than the value ($p/A_V \lesssim 3\%$/mag) observed for the diffuse interstellar space. Theoretically, if highly elongated or flattened shaped grains, e.g. the axial ratio $\gtrsim 2$, are aligned perfectly, the ratio between the polarization degree and the extinction can be higher than the observed value of 9.8 %/mag (e.g. Spitzer 1978, Matsumura and Seki 1996). However, the shape of grains may not be so elongated nor flattened. In addition, it is not clear whether the grains can align or not in the circumstellar space. Thus it seems difficult to explain the observed variation quantitatively by the dichroic extinction.

An alternative explanation is given by assuming the eclipse of the stellar light by orbiting dense clouds and the light scattering by more diffuse circumstellar medium (Grinin 1988). When a dense cloud comes in the line of sight between the star and the observer, the unpolarized stellar light is strongly extinguished, while the scattered light by diffuse medium is less obscured. If the observer cannot resolve the stellar and scattered light, then, the observed net polarization degree increases, while the polarized flux remains almost constant. The polarization degree p_V will vary with the magnitude V as follows:

$$p_V = p_0 10^{0.4(V-V_0)} \tag{5}$$

where p_0 is a constant and expresses the polarization degree at $V = V_0$. A fitted curve by this equation is drawn as the dashed curve in Figure 4. It shows that the polarized flux does not vary in JD= 2449368-2450512. Thus, the variation in this period can be well explained by the eclipse caused by the orbiting clouds.

In the eclipsing model, we may estimate some physical parameters from the photometric data. For all the data, significant variation is apparent in a time scale of $\gtrsim$10 days, but it is not obvious within several days (Table 3). We consider three cases, i.e. (1) the cloud size S_{cl} is much smaller than the stellar radius R_*, (2) S_{cl} is comparable to R_*, and (3) S_{cl} is much larger than R_*.

(1) The case for $S_{cl} \ll R_*$: The stellar flux would not be obscured as to explain the observation, since only the fraction of $(S_{cl}/2R_*)^2$ of the stellar flux would be extinguished even if the cloud is fully opaque. Thus we do not discuss this case.

(2) The case for $S_{cl} \approx R_*$: If the cloud passes over the stellar disk in a time scale τ, the velocity v of the cloud can be written as,

$$v \approx (16\mathrm{km/sec})(\frac{R_*}{10R_\odot})(\frac{\tau}{10\mathrm{days}})^{-1}. \tag{6}$$

The radius of the star R_* is $\approx 10R_\odot$ for a Herbig Ae/Be star (Palla and Stahler 1994). If these clouds are orbiting in a Keplerian motion, the distance r from the star to the clouds can be written as

$$r \approx \frac{GM_*}{v^2} \approx (7\mathrm{AU})(\frac{M_*}{2M_\odot})(\frac{v}{16\mathrm{km/sec}})^{-2}, \tag{7}$$

where M_* is the stellar mass, and G is the gravitational constant. This result shows that the clouds which make eclipse should be very close to the star.

(3) The case for $S_{cl} \gg R_*$: In this case, the time scale obscured by the cloud is determined by S_{cl} and the velocity v of the cloud. Though S_{cl} is not known, we may assume that the size of the cloud S_{cl} is not larger than the circumference of the orbit $2\pi r$ if the orbit is circular. We write the diameter of the cloud as

$$S_{cl} = 2\pi\alpha r \tag{8}$$

where α is a non-dimensional constant with $0 < \alpha < 1$, and the time scale τ obscured by the cloud as,

$$\tau = S_{cl}/v = 2\pi\alpha r/v. \tag{9}$$

If we assume a Keplerian motion, the velocity v of the cloud can be written as

$$v \approx \sqrt{\frac{GM_*}{r}}. \tag{10}$$

Using eqs.(9) and (10), we obtain

$$r \approx (0.11\mathrm{AU})\alpha^{-2/3}(\frac{\tau}{10\mathrm{days}})^{2/3}(\frac{M_*}{2M_\odot})^{1/3}. \tag{11}$$

Since we do not know the value of α, we cannot calculate the proper value of v. However, we can say that the clouds should be present in the vicinity of the star even in this case.

Close et al. 1997 has recently found that R Mon has a companion separated about 670 AU from R Mon, and estimated its period of revolution as about 5×10^3 years. Since the time-scale of the variations discussed in this paper is much shorter, these variations cannot be explained by the companion nor by the grains around it. The clouds which explain our observation should be much closer to R Mon.

The variation in 1991 and 1992 cannot be explained by the model as discussed above, because the polarization flux is smaller than that after 1993 (Fig.4). This variation may be explained if there exists another eclipsing cloud much larger than the extent of the diffuse medium making light scattering. When this cloud passed the line of sight, it would obscure both the stellar and the scattered light. Thus the polarized flux would also decrease.

4.2. Variable Property in Position Angle

The position angle clearly shows temporal variation, but the correlations with other quantities are weak (Table4), and thus it seems difficult to make a general interpretation of its variation. However, we note here a rapid variation of the position angle in 1993. In 1979 or JD$\approx$2444000, a similar rapid variation in the position angle was observed (Scarrott et al. 1989). Figure 7 shows that the variation in 1979 is larger than that in 1993.

It should be noted that the variation in 1993 followed the decrease of the polarized flux in 1991-1992. Similar phenomena, i.e., the decrease of flux and the subsequent variation of the position angle, are also found in another Herbig Ae/Be star WW Vul. In 1987, the polarization degree of WW Vul reached maximum when the flux was minimum, while the position angle changed about 30 days after the flux minimum (Fig.III in Grinin 1994). The time lag between the maximum in polarization degree and that in position angle is fairly shorter than in R Mon. This can be explained if the periastron distance of the orbiting cloud in WW Vul is smaller than that in R Mon.

4.3. Invariable Property in Position Angle

The position angle of R Mon depends on wavelength (Table 2). Since 1965, this property has been observed by various authors (e.g. Fig.9 in Aspin et al. 1985). This dependence is seen even when the position angle happens to change greatly (e.g. Jones and Dyck 1978). This fact cannot be explained by the eclipsing model discussed in Section 4.1, and suggests another mechanism of polarization. A possible explanation is that at least two large clouds are present and scatter off the stellar light. If these clouds have different scattering properties, the contribution to the scattered light will be different at different wavelength. In this model, the invariable dependence of position angle means that the positions of the clouds do not significantly vary during at least in the observed period, i.e. about 30 years, and the periods of their revolution should be much longer. Applying the Kepler's third law, we obtain a restriction for the distance r of the clouds from the star as

$$r \gg (\frac{G}{4\pi^2})^{1/3}(M_*)^{1/3}T^{2/3} \approx (12\mathrm{AU})(\frac{M_*}{2M_\odot})^{1/3}(\frac{T}{30\mathrm{years}})^{2/3}. \tag{12}$$

These clouds should be present in the region far from the clouds which make eclipse.

4.4. More Evidence on Polarization Mechanism

As discussed in Section 4.1, the observed linear polarization is mainly due to the scattered light, and not to the dichroic extinction. This view is further supported by the following points:

(1) The wavelength dependence of polarization in R Mon is completely different from the Serkowski or Wilking law. The polarization degree p increases with wavelength λ (Fig.1). Our results differ from those of Aspin et al. 1985 who showed that the maximum of polarization degree was around the V band, and suggested the dichroic extinction as a mechanism of polarization.

(2) Our PCA shows that the two main components can explain 66 % of the variance in our data (Section 3.2). The first component is the summation of the V magnitude, colors, and the polarization degrees (eq.(3)). It can be interpreted as the effect of the extinction of the stellar light by eclipsing clouds. The meaning of the second component (eq.(4)) is less clear. However, since it includes the position angle θ_V of the polarization, it should be related to the diffuse medium scattering off the stellar light. As this medium moves or its optical properties change, the position angle will also vary. Therefore, our PCA result does not conflict with the view that the observed polarization is mainly due to the scattered light.

(3) Our observation shows that the amount of variation of the V magnitude in the small diaphragm ϕ_1 is smaller than that in the ring-shaped region (Fig.6). If the multiple scattering is assumed near the star in the diffuse medium, the radiation is rather confined there. If the diffuse medium is extended in a disk-shaped region, the variation is hard to propagate in an equatorial direction, while it propagates more easily in the polar direction. Thus, assuming the multiple scattering of light, we may explain the flux variation qualitatively.

Clark and McCall 1997 have developed a single scattering model and suggested light scattering at an optical jet to explain the polarization in the inner $10''$ region. However, our observation does not seem to support it. In their model, the properties of polarization will be different between in the inner region ($\lesssim 10''$) and in the outer region ($\gtrsim 10''$), because the matter which makes scattering is different, i.e. the jet for the inner and cavity walls for the outer regions. However, in our observation, the polarization property is not much different between in the small diaphragm

ϕ_1 (18″) and in the ring-shaped region (18-36″, see Table 1). Furthermore, the variation of the position angle in ϕ_1 is similar to that in the ring-shaped region, and the correlation coefficient is 0.76. These properties suggest that the polarization mechanisms for the inner and outer regions are the same, and it should be close to the star. We favor the view that the light polarized in the vicinity of the star is scattered in the optically thin envelope (Gledhill 1991).

4.5. Variation of Flux - Extinction Curve?

From the variable extinction observed in R Mon, we attempt to investigate the wavelength dependence of the extinction. Since photometric variations are relatively small within a certain period (Table 3), we have averaged the photometric data in Julian Days (a)2448573-2448576, (b)2448951-2449427, (c)2449693-2449742, and (d)2450109-2450407. Figure 8 shows the 'extinction curves' deduced from the difference between (a) and (b) (the circles), and between (c) and (d) (the triangles). Although the decrease of the former curve in $1/\lambda > 2.4\mu\mathrm{m}^{-1}$ is probably due to the scattered light, or 'bluing effect' as discussed earlier, the dependence on the inverse-wavelength for R Mon seems flatter than that for the diffuse interstellar clouds (the long-dashed for $R_V = 3.1$ and short-dashed curves for $R_V = 5.0$, calculated with the formula by Cardelli et al. 1988).

To explain these flattened extinction curves, we performed Mie calculations for spherical grains composed of amorphous carbon ('BE', Rouleau and Martin 1991) and 'astronomical silicate' (Draine 1985) with a power law size distribution. We have changed the upper and lower cutoff sizes, while the power law index was fixed as -3.5. The extinction curve of a 'standard' size distribution of our calculation (radius of the grains $0.001\mu\mathrm{m} < a < 0.25\mu\mathrm{m}$) is similar to that observed for the diffuse clouds or $R_V = 3.1$, as one may expect. When both the upper and lower cutoffs are increased, the curve is flattened. The dot-dashed line in Figure 8 shows the result for the grain radius $0.08\mu\mathrm{m} < a < 0.5\mu\mathrm{m}$, which is similar to the observation. This results indicate that smaller grains may be depleted and larger grains may be present in the clouds around R Mon.

Alternative explanation of the flattened extinction curve is to introduce 'gray' extinction, in addition to the extinction by grains. If the eclipsing clouds are dense and opaque enough, they will throw shadows over the observer. The amount of extinction will then less depend on the wavelength. The dotted curve in Figure 8 shows a mixture of the calculated extinction for $R_V = 5.0$ (Cardelli et al. 1988) and gray extinction, in the proportion of 1 to 0.6 at the V band. It is remarkable that this extinction curve is quite similar to that by the Mie calculation. At the near-infrared wavelength, however, the amount of extinction will be significantly different. Our Mie calculation shows A_K/A_V=0.16 for grains of the radius $0.08\mu\mathrm{m} < a < 0.5\mu\mathrm{m}$, while the model including gray extinction gives A_K/A_V=0.46. Thus observation of the variation at near-infrared is quite important to distinguish these two models.

5. CONCLUSIONS

From our observation of R Mon in 1991-1997, we draw the conclusions as follows:

1. During the observation, the V magnitude changed by about 0.7 mag in ϕ_1. We find positive correlations between V and polarization degree p_V, and between V and colors except $U-B$. These correlations can be explained by the eclipse by dense clouds in the vicinity of the star and the scattering off the stellar light by diffuse medium.

2. We have observed the bluing effect only for the $U-B$ color. Other colors at longer wavelength, i.e. $B-V, V-R_C, V-R_J$, and R_C-I_C, turned red monotonically with decreasing flux.

3. We find that the variation of flux depends on the aperture size of the diaphragm, though the polarization properties do not strongly depend on it. Observationally, this property makes possible to compare the polarimetric data with different diaphragm by different observer. However, much care should be paid to photometric data.

4. The degree of linear polarization increases with wavelength. The dependence on wavelength is completely different from that observed in the diffuse interstellar space, i.e. the Serkowski or the Wilking law.

5. The position angle also depends on wavelength, and it increases by about 5 degrees from 0.36 to 0.76 μm. This property is rather time-independent compared with the flux variation. This fact suggests that the region where the stellar light is scattered is more extended than the region where the eclipsing clouds exist.

6. On the assumption that the variation of the flux is due to extinction, we attempt to draw extinction curve from our data. The drawn curve seems flatter than the calculated one for $R_V = 5$. This curve may be explained by grains of a size distribution ranging from 0.08 to 0.5 μm, or by the mixture of extinction by grains and gray extinction.

Note added in proof: Voshchinnikov et al (AA 312, 243, 1996) calculated the light scattering around young stellar objects with Monte Carlo simulations, and showed that the small grains are depleted in the circumstellar dust shells for AB Aur, HD 25931, and HD200775.

We are grateful to the staff of Dodaira Observatory for assistance of the observations. We also acknowledge S. Kikuchi for his advice on the observational method when we started the observation. R. Hirata is acknowledged for the information about photometric reduction. This work was partly supported by the Grant-in-Aid for the Scientific Research (No.08740174) of the Japanese Ministry of Education, Culture, Sports, and Science.

A. TRANSFORMATION TO STANDARD PHOTOMETRIC SYSTEM

We used the following formulae to convert our data into values in the standard system (Hirata 1992, private communication):

$$V = m_4 + C_1$$

$$U - B = 0.84(m_1 - m_3) + C_2$$

$$B - V = 1.47(m_3 - m_4) + C_3$$

$$V - R_C = 0.82(m_4 - m_5) + C_4$$

$$V - R_J = 0.94(m_4 - m_6) + C_5$$

$$R_C - I_C = 1.25(m_5 - m_7) + C_6,$$

where m_i denotes the magnitude with the i-th photomultiplier. The adopted effective wavelengths are 0.36, 0.42, 0.455, 0.53, 0.64, 0.69, and 0.76 μm for the channel 1 to 7, respectively. The factors in the equations are calculated from the difference between the effective wavelength in our system and that in the standard one. By observing photometric standard stars, Hirata (1997, private communication) obtained the results which were slightly different from the above formulae. However, the results using transformation by Hirata(1997) will not differ no more than 0.05 mag in the V magnitude nor in the colors for R Mon.

Table 1. Photometric Properties of Comparison Stars

···	SAO114210(=C_1)	HD251389(=C_2)
V	9.43 ± 0.02	10.40 ± 0.02
U-B	-0.05 ± 0.02	0.00 ± 0.02
B-V	0.01 ± 0.02	0.43 ± 0.02
V-R_C	0.02 ± 0.03	0.27 ± 0.03
V-R_J	0.06 ± 0.06	0.46 ± 0.06
R_C-I_C	0.00 ± 0.04	0.22 ± 0.04

Table 2. Time Averages for 26 Observations in 1991-1997

	$\phi_1(18'')$	$\phi_2(36'')$	Ring$(\phi_1 - \phi_2)$
$p(0.360\mu\mathrm{m})$ (%)	10.25 ± 0.29	9.31 ± 0.45	8.70 ± 0.69
$p(0.420\mu\mathrm{m})$ (%)	10.37 ± 0.28	9.45 ± 0.26	8.39 ± 0.43
$p(0.455\mu\mathrm{m})$ (%)	10.35 ± 0.24	9.50 ± 0.21	8.45 ± 0.31
$p(0.530\mu\mathrm{m})$ (%)	11.30 ± 0.29	10.28 ± 0.27	8.93 ± 0.34
$p(0.640\mu\mathrm{m})$ (%)	10.46 ± 0.29	10.23 ± 0.26	8.47 ± 0.39
$p(0.690\mu\mathrm{m})$ (%)	12.17 ± 0.34	11.16 ± 0.27	9.64 ± 0.31
$p(0.760\mu\mathrm{m})$ (%)	12.04 ± 0.38	10.89 ± 0.32	9.28 ± 0.48
p_V(%)	11.24 ± 0.12	10.21 ± 0.11	8.90 ± 0.15
a(%μm)	-1.43 ± 0.24	-1.43 ± 0.25	-0.83 ± 0.36
$\theta(0.360\mu\mathrm{m})$ (deg)	83.48 ± 1.03	86.16 ± 1.18	92.61 ± 2.87
$\theta(0.420\mu\mathrm{m})$ (deg)	86.08 ± 0.79	88.46 ± 0.75	93.19 ± 1.40
$\theta(0.455\mu\mathrm{m})$ (deg)	85.97 ± 0.85	87.89 ± 0.91	91.33 ± 1.28
$\theta(0.530\mu\mathrm{m})$ (deg)	88.10 ± 0.93	90.32 ± 0.80	94.82 ± 0.99
$\theta(0.640\mu\mathrm{m})$ (deg)	88.60 ± 0.97	91.06 ± 0.86	97.08 ± 0.96
$\theta(0.690\mu\mathrm{m})$ (deg)	89.23 ± 1.03	91.57 ± 0.92	97.11 ± 1.14
$\theta(0.760\mu\mathrm{m})$ (deg)	88.67 ± 1.05	91.54 ± 0.95	98.89 ± 2.15
θ_V (deg)	87.62 ± 0.37	90.02 ± 0.35	95.24 ± 0.48
b (deg μm)	-3.75 ± 0.77	-3.74 ± 0.79	-5.68 ± 1.34
V (mag)	12.02 ± 0.04	11.48 ± 0.05	12.50 ± 0.06
$U - B$ (mag)	-0.16 ± 0.02	-0.16 ± 0.02	-0.16 ± 0.02
$B - V$ (mag)	0.64 ± 0.02	0.59 ± 0.02	0.53 ± 0.02
$V - R_C$ (mag)	0.63 ± 0.03	0.57 ± 0.03	0.51 ± 0.03
$V - R_J$ (mag)	0.85 ± 0.06	0.83 ± 0.06	0.63 ± 0.07
$R_C - I_C$ (mag)	0.43 ± 0.04	0.37 ± 0.04	0.24 ± 0.05

Note. — The errors listed are 1σ dispersions of the means. a and b are defined by eqs.(1) and (2), respectively.

Table 3. Temporal Variation for the Quantities Observed with ϕ_1

Date[a]	p_V	a	θ_V	b	V	$U-B$	$B-V$	$V-R_C$	$V-R_J$	R_C-I_C
8573.80	12.6(0.1)	-1.3(0.3)	86.5(0.3)	-4.4(0.7)	12.41(0.03)	-0.22(0.04)	0.77(0.04)	0.68(0.04)	0.98(0.07)	0.54(0.09)
8574.80	12.3(0.3)	-0.6(0.6)	87.1(0.6)	-3.2(1.3)	...	...	...	...	...	...
8575.80	12.6(0.2)	-2.2(0.4)	87.0(0.4)	-3.9(0.9)	12.45(0.02)	-0.21(0.03)	0.77(0.04)	0.69(0.03)	0.99(0.06)	0.52(0.06)
8576.79	12.8(0.2)	-1.3(0.4)	87.8(0.4)	-3.5(1.0)	12.43(0.02)	-0.25(0.03)	0.74(0.03)	0.68(0.03)	0.95(0.06)	0.48(0.09)
8951.80	9.4(0.2)	-0.7(0.4)	84.7(0.5)	-3.0(1.1)	12.03(0.02)	-0.20(0.02)	0.63(0.03)	0.64(0.03)	0.91(0.06)	0.42(0.05)
8952.80	9.4(0.1)	-1.1(0.3)	85.7(0.4)	-4.3(0.9)	11.97(0.02)	-0.16(0.02)	0.51(0.02)	0.62(0.03)	0.88(0.06)	0.43(0.06)
8953.80	9.4(0.1)	-1.4(0.3)	84.5(0.4)	-3.9(0.8)	12.01(0.02)	-0.11(0.02)	0.52(0.02)	0.65(0.03)	0.92(0.06)	0.45(0.04)
9005.59	10.0(0.1)	-1.6(0.3)	88.4(0.4)	-2.0(0.8)	11.95(0.02)	-0.18(0.03)	0.66(0.03)	0.66(0.03)	0.94(0.06)	0.43(0.05)
9368.61	11.5(0.2)	-2.3(0.4)	81.7(0.4)	-3.4(1.0)	12.06(0.02)	-0.17(0.02)	0.66(0.02)	0.66(0.03)	0.93(0.06)	0.41(0.04)
9372.58	11.6(0.1)	-1.5(0.3)	80.9(0.3)	-2.4(0.9)	12.02(0.02)	-0.15(0.03)	0.68(0.03)	0.65(0.03)	0.93(0.06)	0.43(0.05)
9398.55	11.2(0.1)	-1.8(0.3)	81.5(0.3)	-4.4(0.8)	11.94(0.03)	-0.17(0.04)	0.66(0.04)	0.63(0.04)	0.91(0.06)	0.44(0.06)
9400.60	11.4(0.2)	-1.9(0.4)	80.6(0.4)	-1.7(1.0)	11.94(0.03)	-0.16(0.03)	0.69(0.04)	0.65(0.03)	0.92(0.06)	0.43(0.05)
9427.55	11.2(0.1)	-2.0(0.3)	79.8(0.3)	-1.8(0.9)	11.98(0.02)	-0.17(0.03)	0.65(0.03)	0.62(0.03)	0.88(0.06)	0.43(0.04)
9693.76	9.2(0.1)	-0.7(0.3)	88.2(0.3)	-4.5(0.8)	11.80(0.02)	-0.21(0.02)	0.61(0.02)	0.60(0.03)	0.86(0.06)	0.40(0.04)
9696.75	8.8(0.1)	-1.6(0.2)	89.5(0.3)	-3.1(0.7)	11.74(0.02)	-0.22(0.02)	0.61(0.02)	0.59(0.03)	0.86(0.06)	0.40(0.04)
9738.46	9.3(0.2)	-2.0(0.4)	87.4(0.5)	-10.7(1.4)	11.77(0.03)	-0.19(0.04)	0.63(0.04)	0.59(0.03)	0.88(0.06)	0.41(0.05)
9739.50	9.8(0.2)	-0.8(0.5)	89.1(0.5)	-8.7(1.4)	11.77(0.02)	-0.18(0.04)	0.60(0.04)	0.59(0.03)	0.88(0.06)	0.43(0.05)
9741.54	10.1(0.2)	-0.8(0.5)	89.4(0.5)	-7.9(1.3)	11.77(0.02)	-0.20(0.03)	0.61(0.03)	0.58(0.03)	0.87(0.06)	0.25(0.05)
9742.55	10.0(0.1)	-0.8(0.3)	89.3(0.3)	-8.8(0.8)	11.83(0.02)	-0.16(0.02)	0.62(0.02)	0.61(0.03)	0.89(0.06)	0.41(0.04)
10042.80	10.9(0.2)	-2.7(0.5)	89.2(0.5)	-2.6(1.3)	...	...	...	...	...	...
10108.63	12.0(0.3)	-1.3(0.7)	89.0(0.8)	0.9(1.8)	12.09(0.02)	...	0.59(0.03)	0.64(0.02)	0.93(0.06)	0.44(0.07)
10109.66	11.8(0.1)	-2.1(0.4)	86.6(0.3)	-3.2(0.9)	12.08(0.02)	-0.16(0.03)	0.62(0.03)	0.61(0.03)	0.91(0.06)	0.45(0.04)
10110.67	12.5(0.2)	-1.9(0.4)	87.2(0.4)	-2.0(1.0)	12.09(0.02)	-0.15(0.04)	0.64(0.04)	0.62(0.03)	0.91(0.06)	0.44(0.05)
10127.61	12.2(0.2)	-2.3(0.6)	89.4(0.6)	-0.8(1.4)	11.98(0.04)	-0.14(0.05)	0.65(0.06)	0.60(0.04)	0.88(0.07)	0.44(0.07)
10403.71	12.2(0.2)	-2.6(0.5)	91.9(0.4)	-3.6(1.1)	12.13(0.02)	-0.10(0.04)	0.65(0.04)	0.62(0.03)	0.90(0.06)	0.41(0.05)
10407.77	12.7(0.2)	-1.2(0.5)	91.9(0.4)	-1.1(1.1)	12.14(0.03)	-0.08(0.04)	0.63(0.04)	0.60(0.03)	0.89(0.06)	0.43(0.06)
10484.56	12.8(0.2)	-2.5(0.5)	95.4(0.4)	-6.3(1.1)	12.07(0.04)	-0.06(0.09)	0.62(0.10)	0.61(0.05)	0.88(0.08)	0.39(0.09)
10486.54	13.1(0.2)	-2.7(0.4)	94.6(0.3)	-6.6(0.9)	12.05(0.04)	-0.04(0.05)	0.63(0.06)	0.61(0.05)	0.88(0.07)	0.42(0.06)
10512.50	14.1(0.2)	-1.8(0.5)	98.2(0.4)	-9.2(1.0)	12.14(0.03)	-0.03(0.06)	0.66(0.05)	0.63(0.04)	0.90(0.06)	0.43(0.06)

Note. — The numbers in parenthesis are 1σ dispersions. a and b are defined by eqs.(1) and (2), respectively.

[a] Julian Day - 2440000.

Table 4. Correlation Coefficients between Observed Quantities

$\cdots$	V	U-B	B-V	V-R_C	V-R_J	R_C-I_C	p_V	a	θ_V	b
V	$\cdots$	0.02	0.67	0.77	0.81	0.72	0.73	-0.28	0.05	0.32
U-B	0.02	$\cdots$	-0.28	-0.23	-0.24	-0.07	0.47	-0.40	0.49	-0.09
B-V	0.67	-0.28	$\cdots$	0.63	0.69	0.50	0.61	-0.28	-0.06	0.17
V-R_C	0.77	-0.23	0.63	$\cdots$	0.94	0.71	0.37	-0.14	-0.33	0.33
V-R_J	0.81	-0.24	0.69	0.94	$\cdots$	0.71	0.43	-0.16	-0.27	0.27
R_C-I_C	0.72	-0.07	0.50	0.71	0.71	$\cdots$	0.42	-0.24	-0.12	0.28
p_V	0.73	0.47	0.61	0.37	0.43	0.42	$\cdots$	-0.53	0.31	0.17
a	-0.28	-0.40	-0.28	-0.14	-0.16	-0.24	-0.53	$\cdots$	-0.03	-0.22
θ_V	0.05	0.49	-0.06	-0.33	-0.27	-0.12	0.31	-0.03	$\cdots$	-0.43
b	0.32	-0.09	0.17	0.33	0.27	0.28	0.17	-0.22	-0.43	$\cdots$

REFERENCES

Aspin, C., McLean, I. S., and Coyne, G. V. 1985, A&A, 149, 158

Bastien, P. and Ménard F. 1990, ApJ, 326, 334

Bastien, P. and Ménard F. 1990, ApJ, 364, 232

Cardelli, J. A., Clayton, G. C., and Mathis, J. S. 1984, ApJ, 329, L33

Clark, S. and McCall, A. 1997, MNRAS, 284, 513

Close, L. M., Roddier, F., Hora, J., Northcott, M., Roddier, C., Graves, J. E., Hoffmann, W. F., Dayal, A., Fazio, G. G., Deutsch, L. K. 1997, ApJ, 489, 210

Draine, B. T. 1985, ApJS, 57, 587

Fischer, O., Henning, Th., Yorke, H. W. 1994, A&A, 284, 187

Fischer, O., Henning, Th., Yorke, H. W. 1996, A&A, 308, 863

Garrison, L. M. and Anderson C. M. 1978, ApJ, 221, 601

Gledhill, T. M. 1991, MNRAS, 252, 138

Grinin, V. P. 1988, Pis'ma Astron. Zh., 14, 65

Grinin, V. P. 1994, in The Nature and Evolutionary Status of Herbig Ae/Be Stars, ed. P. S. Thé, M. R. Pérez, & E. P. J. van den Heuvel (Astronomical Society of the Pacific) p.63

Hall, R. C. 1964, ApJ, 139, 759.

Hall, R. C. 1965, PASP, 77, 158.

Herbig, G. H. and Bell, K. R., 1988, Lick Observatory Bulletin No.1111

Hsu, J. and Breger, M., 1982, ApJ, 262, 732

Jones T. J. and Dyck H. M. 1978, ApJ, 220, 159

Khatchikyan, E. E., 1958, Soob. Biurakanskoi Obs. 25, 67

Kikuchi, S. 1988, Tokyo Astron. Bull. Ser. II, 281, 3267

Lightfoot, J. F., 1989, MNRAS, 239, 665

Matsumura, M. and Seki, M. 1995, Ap&SS, 224, 513

Matsumura, M. and Seki, M. 1996, ApJ, 456, 557

Matsumura, M., Seki, M., and Kawabata, K. 1998, in Pulsation Stars: Recent Developments in Theory and Observation, ed. M. Takeuti and D. D. Sasselov (Tokyo: Universal Academy Press) p.107

Ménard, F., Bastien, P., and Robert, C. 1988, ApJ, 335, 290

Minchin, N. R., Hough, J. H., McCall, A., Aspin, C., Yamashita, T., and Burton, M. G. 1991, MNRAS, 249, 707

Moffett, T. J. and Barnes, T. G. 1979, AJ, 84, 627

Hutchinson, M. G., Albinson, J. S., Barrett, P., Davies, J. K., Evans, A., Goldsmith, M. J., and Maddison, R. C. 1994, A&A, 285, 883

Palla, F., and Stahler, S. W. in The Nature and Evolutionary Status of Herbig Ae/Be Stars, ed. P. S. Thé, M. R. Pérez, & E. P. J. van den Heuvel (Astronomical Society of the Pacific) p.391

Razmadze, N. A., 1959, Bull. Abastumani Astrophys. Obs. 24, 25

Rouleau, F., and Martin P. G. 1991, ApJ, 377, 526

Scarrott, S. M., Draper, P. W., and Warren-Smith, R. F. 1989, MNRAS, 237, 621

Serkowski, K. 1974, in Planets, Stars and Nebulae Studied with Photopolarimetry, ed. T. Gehrels (Tucson: University of Arizona) p.135

Spitzer, L. Jr. 1978, Physical Processes in the Interstellar Medium (John Wiley & Sons)

Thé, P. S., de Winter, D., and Pérez, M. R. 1994, A&AS, 104, 315

Vrba, F. J., Schmidt, G. D. and Hintzen, P. M. 1979, ApJ, 227, 185

Walker M. F. 1956, ApJS, 2, 365

Warren-Smith, R.F., Draper, P. W., and Scarrott, S. M. 1987, ApJ, 315, 500

Whitney, B. A. and Hartmann, L. 1992, ApJ, 395, 529

Whitney, B. A. and Hartmann, L. 1993, ApJ, 402, 605

Zellner B. 1970, AJ, 75, 182

This preprint was prepared with the AAS LaTeX macros v4.0.

Fig. 1.— The dependence of polarization degree p and position angle θ on the inverse wavelength $1/\lambda$ for the $18''$ diaphragm (ϕ_1). The data in one observational season are averaged. The filled circles show the average in November 1991 (Julian Day is from 2448573 to 2448576, 4 nights), the open circles in 1992-93 (JD is from 2448951 to 2449005, 4 nights), the filled triangles in 1993-94 (JD is from 2449368 to 2449427, 5 nights), the open triangles in 1994-95 (JD is from 2449693 to 2449742, 6 nights), the filled squares in 1995-96 (JD is from 2450042 to 2450127, 4 nights), the open squares in November 1996 (JD is from 2450403 to 2450409, 3 nights), and the asterisks in February and March 1997 (JD is from 2450484 to 2450512, 3 nights).

Fig. 2.— The time dependence of (a) the V magnitude, (b) the $B-V$ color, (c) the polarization degree p_V, and (d) the position angle θ_V. The filled circles in (a) show the magnitude in the $18''$diaphragm (ϕ_1), while the open circles show that in the ring-shaped region.

Fig. 3.— Time variation of the V band polarization in a QU plane. The symbols showing the observational period are the same as in Figure 1. Error bars are shown only for the data in February and March 1997.

Fig. 4.— The correlation between the V magnitude and the polarization degree p_V. The symbols show the observation period, same as in Figure 1. The dotted line is a linear fit for the data after JD=2449368, while the dashed curve is the result of fitting with eq.(5) for the same data. See text for the detail.

Fig. 5.— The color-magnitude diagrams. (a) $U-B$ v.s. V. (b) $B-V$ v.s. V. (c) $V-R_C$ v.s. V. (c) R_C-I_C v.s. V.

Fig. 6.— The comparison of the V magnitude in ϕ_1 with that in the ring-shaped region. The dotted line is the result of linear fitting. Its inclination is 1.33.

Fig. 7.— The polarization degree and position angle of R Mon from 1964 to 1997 in the V band. The data are cited from different authors (Julian day of observation - reference): 2438738 - Hall (1965), ~2440200-~2440530 - Zellner (1970), ~2441960-~2441990 - Vrba et al. (1979), 2442803 - Garrison and Anderson (1978), ~2443000 - Jones and Dick (1978), 2445650 - Aspin et al. (1985), 2446431 - Scarrott et al. (1989), and 2448573-2450512 - this paper.

Fig. 8.— The 'extinction curves' derived from the variable flux. The filled circles show the 'curve' obtained from difference between the flux from JD= 2448573-2448576 and that in JD=2448951-2449427. The filled triangles are plotted with the data obtained from the flux in JD=2449693-2449742 and that in JD=2450109-2450407. With using an analytic expression by Cardelli et al. (1988), the long-dashed curve is drawn for $R_V = 3.1$, while the short-dashed curve is for $R_V = 5.0$. The results of Mie calculations are presented as the dot-dashed curve for the grain radius $0.08\mu\text{m} < a < 0.50\mu\text{m}$. The dotted curve shows the extinction by the mixture of extinction with $R_V = 5.0$ (Cardelli et al. 1988) and gray extinction, in the proportion of 1 to 0.6 at the V band.

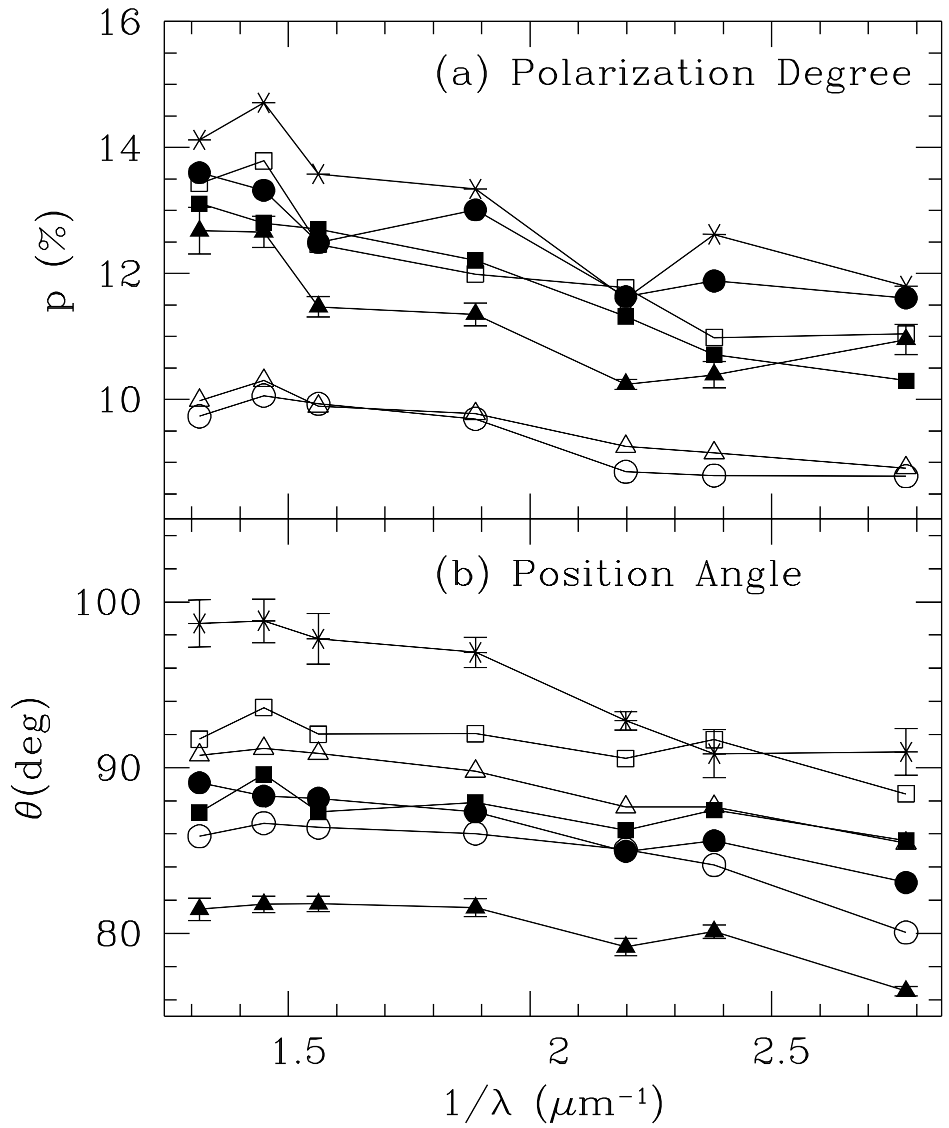
(a) Polarization Degree
p (%)
16
14
12
10
(b) Position Angle
θ(deg)
100
90
80
1.5
2
2.5
1/λ (μm⁻¹)

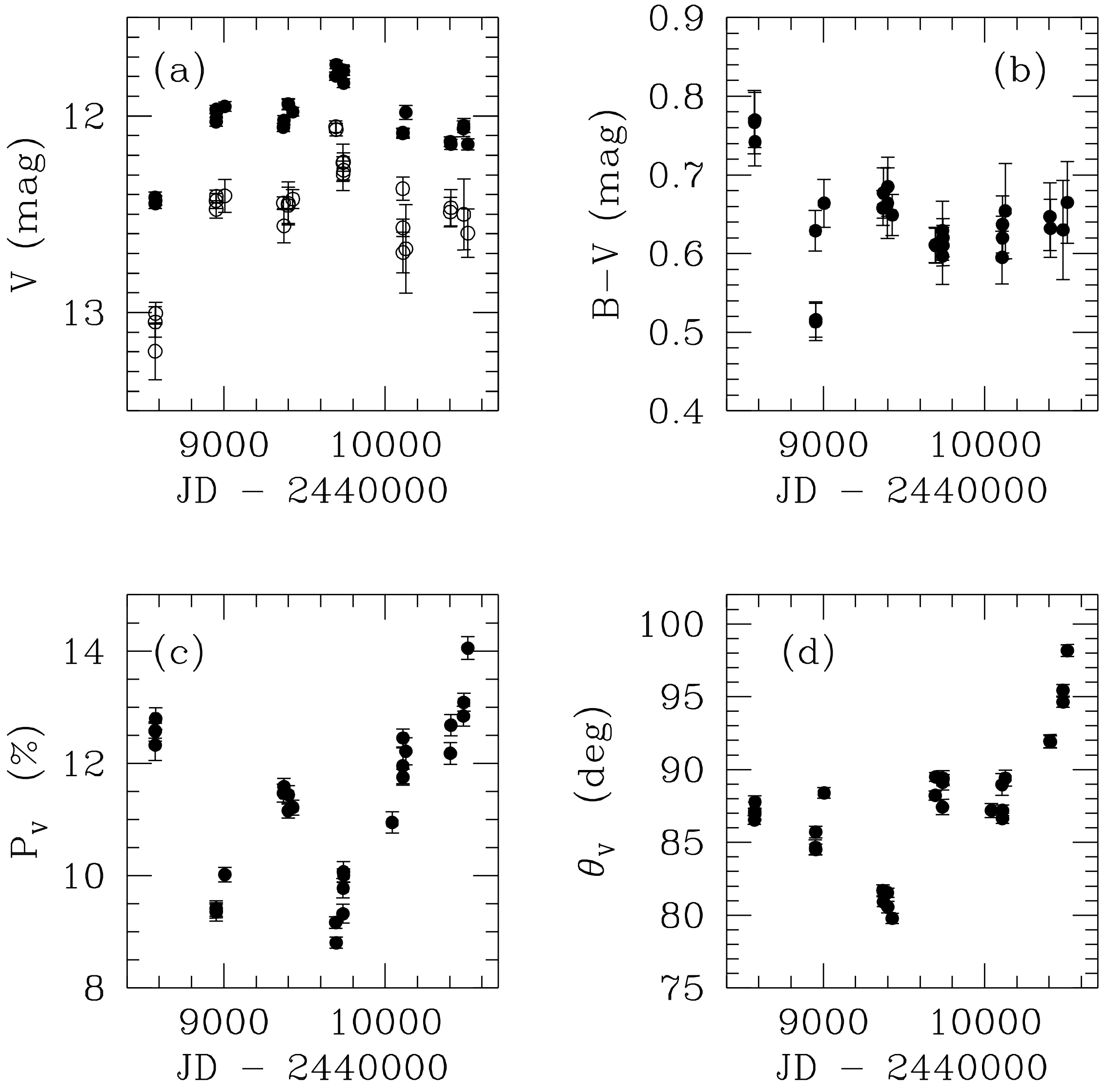
(a)
V (mag)
12
13
9000
10000
JD − 2440000
(b)
B−V (mag)
0.9
0.8
0.7
0.6
0.5
0.4
9000
10000
JD − 2440000
(c)
P_V (%)
14
12
10
8
9000
10000
JD − 2440000
(d)
θ_V (deg)
100
95
90
85
80
75
9000
10000
JD − 2440000

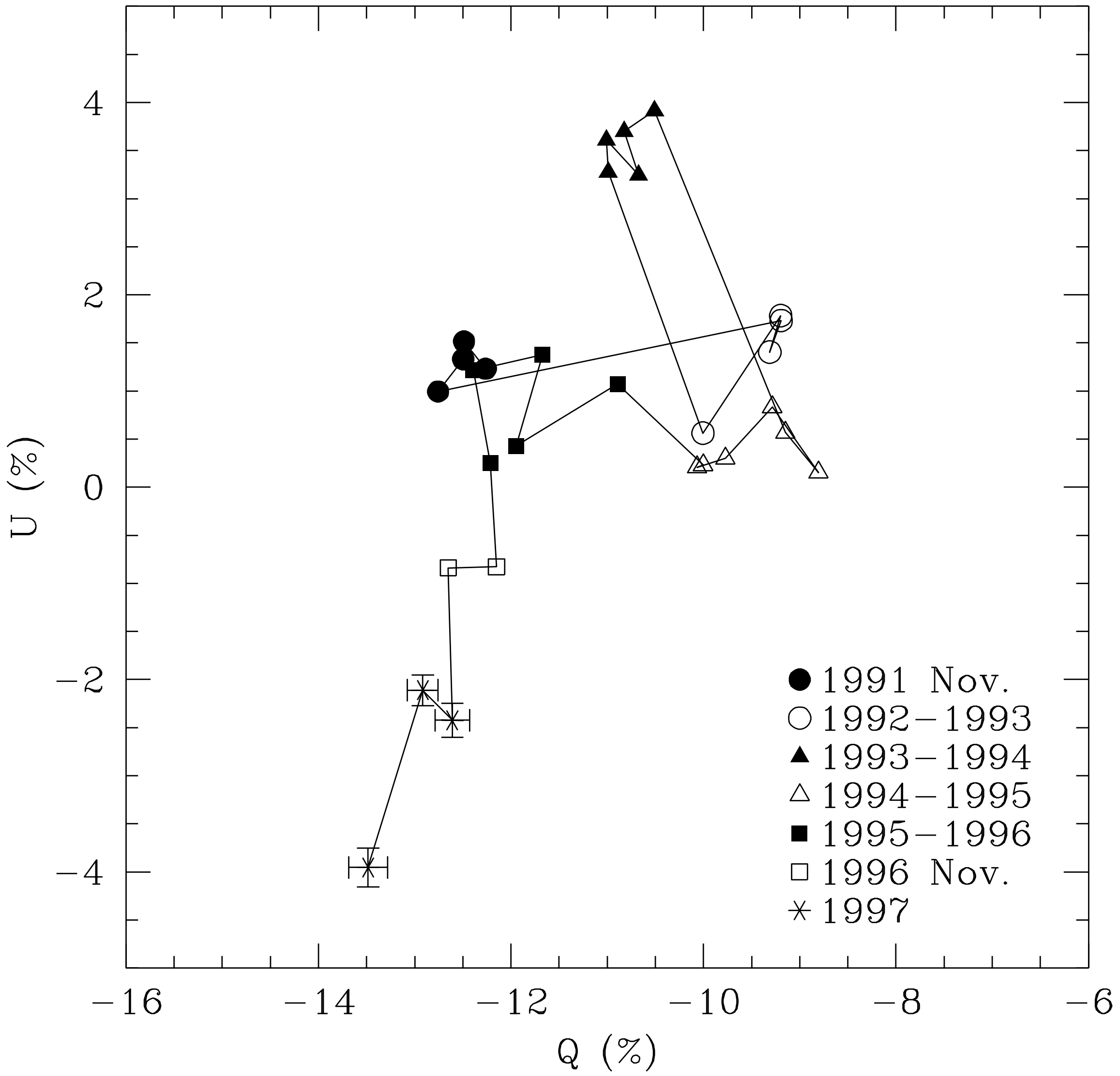
4
2
0
−2
−4
U (%)
−16
−14
−12
−10
−8
−6
Q (%)
1991 Nov.
1992−1993
1993−1994
1994−1995
1995−1996
1996 Nov.
1997

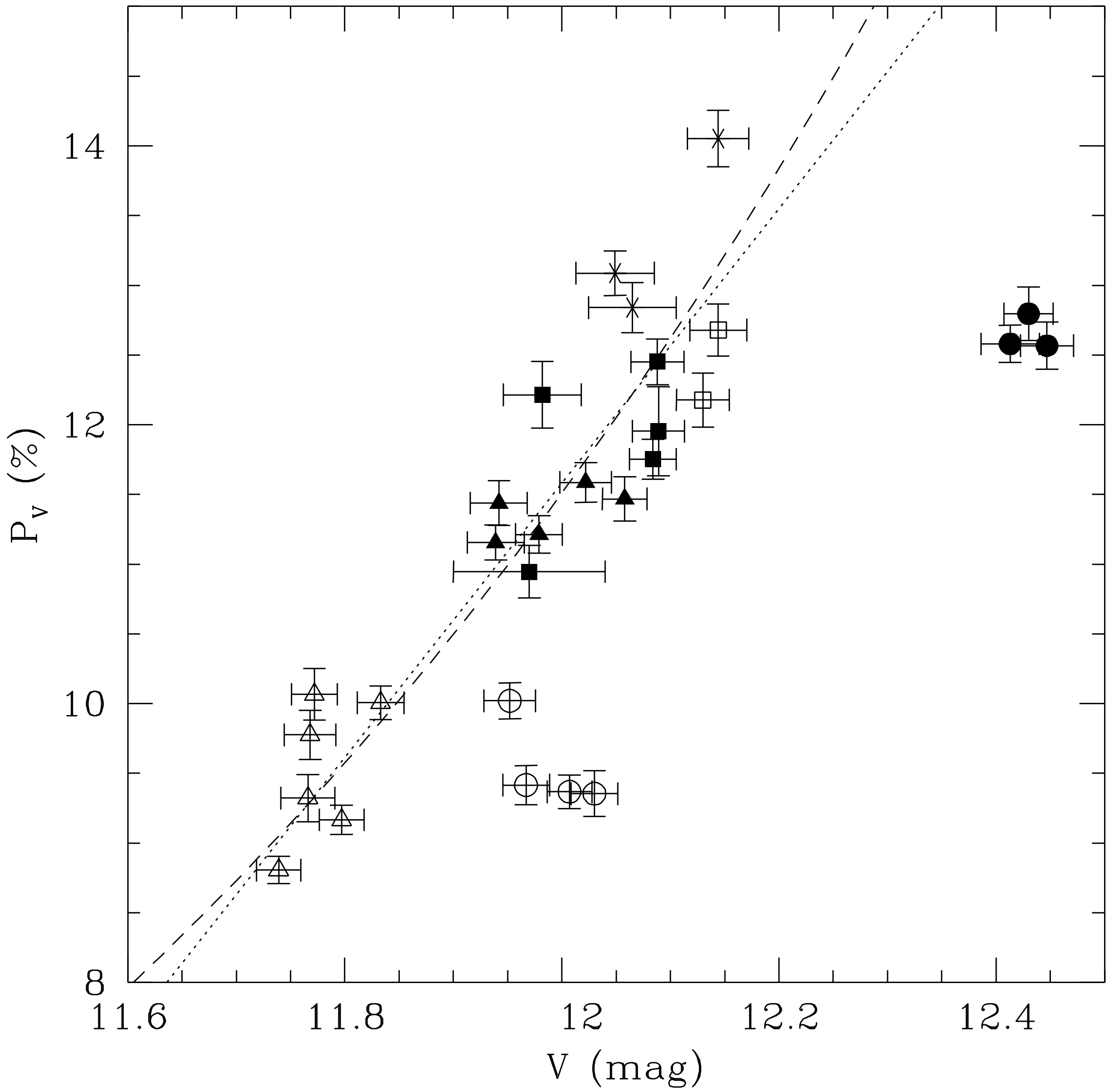
14
12
10
8
11.6
11.8
12
12.2
12.4
P_V (%)
V (mag)

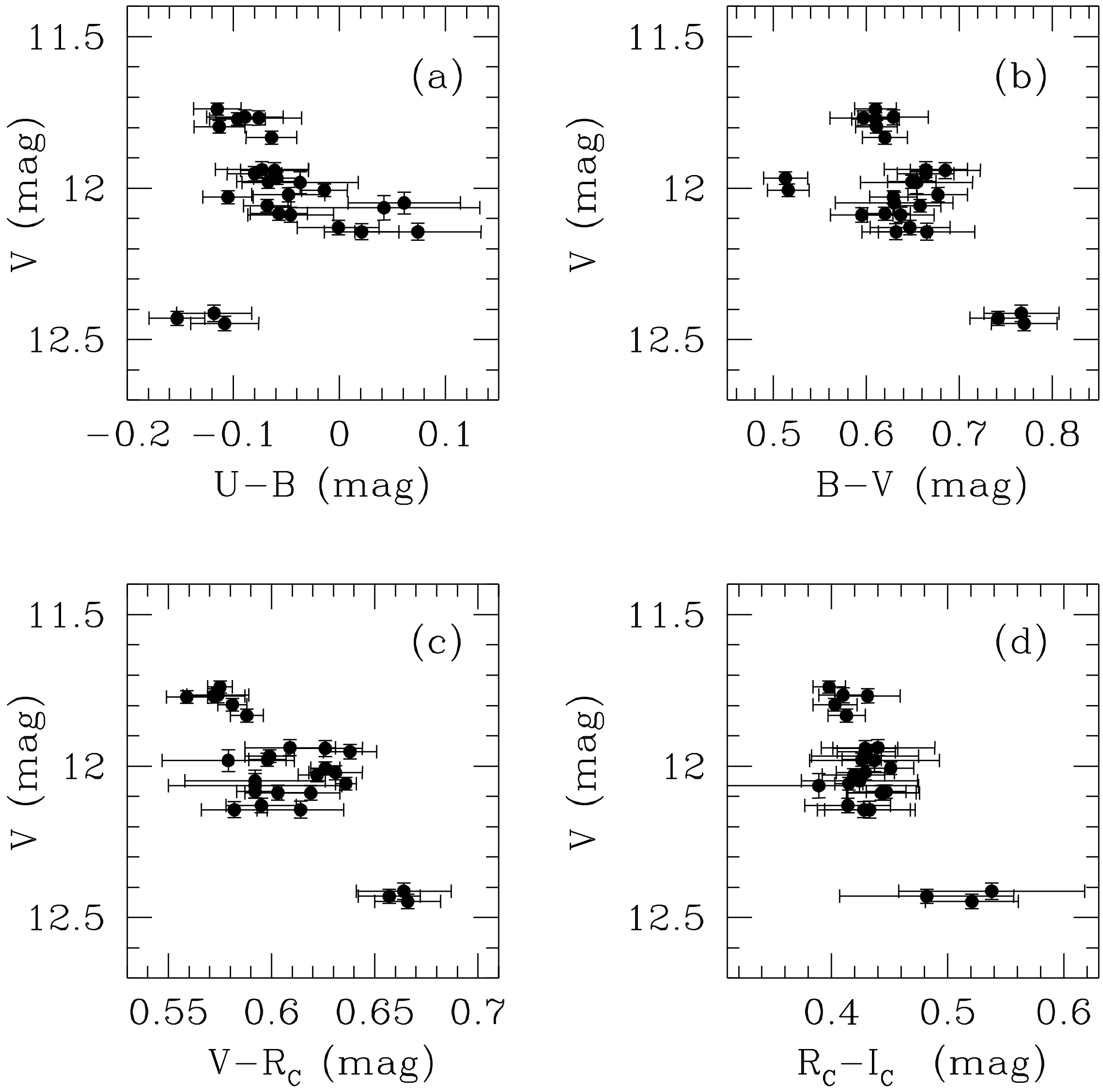
(a)
(b)
(c)
(d)
V (mag)
11.5
12
12.5
−0.2
−0.1
0
0.1
U−B (mag)
0.5
0.6
0.7
0.8
B−V (mag)
0.55
0.6
0.65
0.7
V−R$_c$ (mag)
0.4
0.5
0.6
R$_c$−I$_c$ (mag)

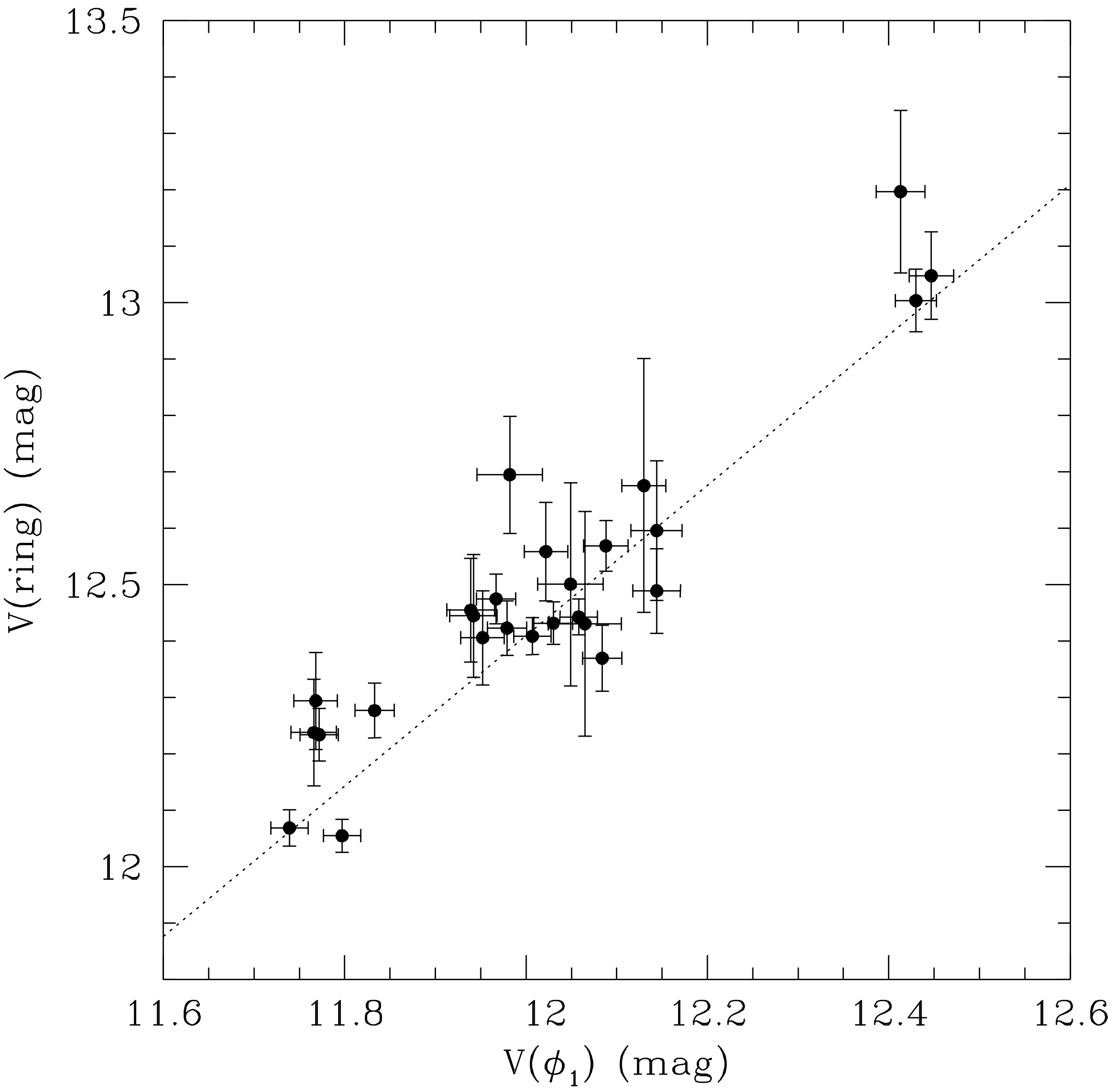
13.5
13
12.5
12
V(ring) (mag)
11.6
11.8
12
12.2
12.4
12.6
V(ϕ_1) (mag)

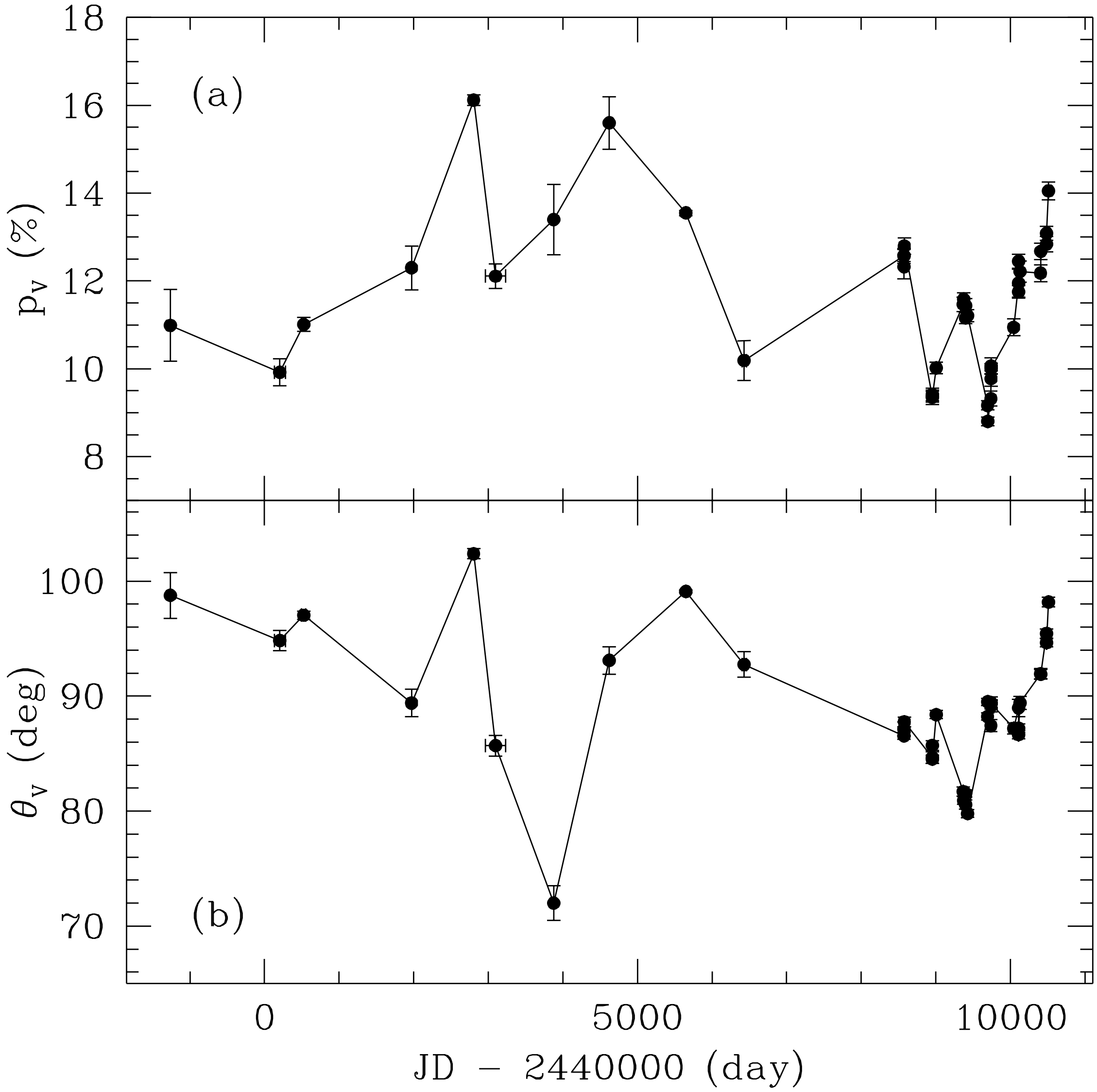
18
16
14
12
10
8
(a)
p_V (%)
100
90
80
70
(b)
θ_V (deg)
0
5000
10000
JD – 2440000 (day)

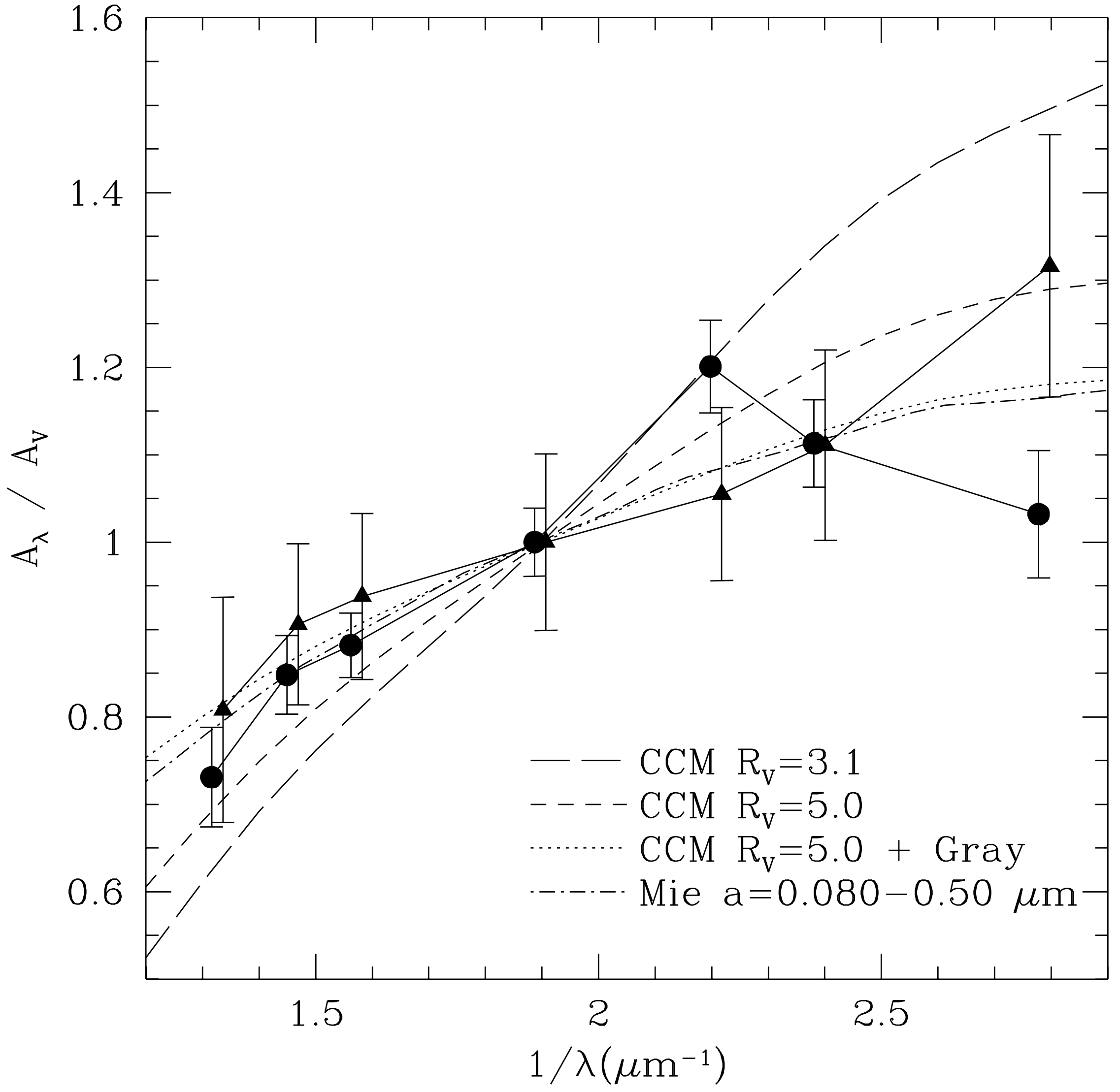
1.6
1.4
1.2
1
0.8
0.6
A_λ / A_V
1.5
2
2.5
$1/\lambda(\mu m^{-1})$
CCM R_V=3.1
CCM R_V=5.0
CCM R_V=5.0 + Gray
Mie a=0.080−0.50 μm